Pattern Recognition 173 (2026) 112808

Contents lists available at ScienceDirect

Pattern Recognition

journal homepage: www.elsevier.com/locate/pr

FPQuant: A deep learning-based scalable framework for fingerprint phenomics quantification in large-scale biometric population studies

Zhiyong Han [a,†], Yelin Shi [b,†], Zhao Zhang [b], Mu Li [c], Haiguo Zhang [c], Jingze Tan [c], Wentian Zhen [c], Tingting Liu [a], Xueying Wang [a], Chengyan Wang [a], Jiucun Wang [a], Li Jin [a], Sijia Wang [d,*], Manhua Liu [b,*], Jinxi Li [a,*]

[a] State Key Laboratory of Genetics and Development of Complex Phenotypes, Collaborative Innovation Center for Genetics and Development, Human Phenome Institute, School of Life Sciences, and Zhang jiang Fudan International Innovation Center, Fudan University, Shanghai 200433, China
[b] School of Electronic Information and Electrical Engineering, Shanghai Jiao Tong University, Shanghai 200240, China
[c] Ministry of Education Key Laboratory of Contemporary Anthropology, Department of Anthropology and Human Genetics, School of Life Sciences, Fudan University, Shanghai 200438, China
[d] CAS Key Laboratory of Computational Biology, Shanghai Institute of Nutrition and Health, University of Chinese Academy of Sciences, Chinese Academy of Sciences, Shanghai 200031, China

ARTICLE INFO

Keywords:
Anthropology
Fingerprint classification
Singularity detection
Morphometric quantification
Deep learning
Pattern recognition

ABSTRACT

Fingerprint morphology, while evolutionary conserved yet individually distinct, emerges as a pivotal biometric identifier in anthropological research and forensic investigation. Current methodologies for precise identification and quantification of complex morphological features—particularly ridge counting and mean ridge-furrow pairs ridge breadth—remain constrained by labor-intensive and monolithic pattern recognition systems. This study presents FPQuant (Fingerprint Phenomics Quantification), a multi-task deep learning framework integrating the most comprehensive fingerprint pattern classification, singularity detection, and quantification of 12 morphometric phenotypes to date. Leveraging NSPT database of 28,867 expert-curated fingerprints, FPQuant achieved state-of-the-art performance with 97.18 % (6-class), 98.62 % (5-class), and 98.67 % (4-class) pattern classification accuracy; 98.63 % precision in topological singularity detection through optimized discrete keypoint localization; and expert-level precision in critical quantitative measurements including ridge counting. Cross-database validation demonstrated extraordinary generalizability with 96.20 % of 5-class accuracy on NIST-4 and 97.75 % of singularity precision on FVC2002 DB1. Notably, FPQuant's integrated phenotypic capability revealed uncharacterized geographic variation in six morphometric traits, establishing novel fingerprint morphometric biomarkers for anthropological research. This study creates a scalable technical paradigm that bridging fingerprint phenomics with large-scale population study, while providing potential new research avenues across anthropology, forensics and biometric authentication.

1. Introduction

Fingerprints, characterized by parallel furrows and ridges on fingertips, exhibit phenotypic diversity shaped by both genetic determinants and early prenatal environmental factors [1,2]. These regular configurations form three principal pattern types: arch, loop, and whorl, which can be further sub-classified into three, four, five and six categories (Fig. 1A). These primary patterns are highly distinctive and persistent, forming a stable basis for individual identification and population studies [3]. Morphometric features such as ridge count, ridge density and major axis angle capture heritable variations linked to sex [4], geographic distance, racial and ethnic variations [5], and developmental asymmetry [6]. However, the identification and quantification of fingerprint phenotypes remain a challenge in large-scale population studies. In particular, measuring fingerprints—especially regarding morphometric phenotypes (e.g., ridge counts, breadth, and density; Table 1)—predominantly relies on manual methods or low-precision techniques, thereby severely limiting reproducibility and

* Corresponding authors.
E-mail addresses: wangsijia@sinh.ac.cn (S. Wang), mhliu@sjtu.edu.cn (M. Liu), lijinxi@fudan.edu.cn (J. Li).
† Contributed equally to this work.

https://doi.org/10.1016/j.patcog.2025.112808
Received 15 May 2025; Received in revised form 21 November 2025; Accepted 28 November 2025
Available online 1 December 2025

hindering a comprehensive, multidimensional analysis of fingerprint phenotypic heterogeneity across extensive populations.

Current fingerprint pattern classification methods primarily encompass conventional approaches based on syntax, singularity, and structure, as well as deep learning methods utilizing convolutional neural networks (CNNs) [7,8]. Syntax-based methods rely on grammar classification, singularity-based methods extract flow-line traces from singular regions, and structure-based methods use inexact graph matching to construct relational graphs from directional image segmentation. Despite achieving a maximum accuracy of 91.60 % on the NIST-4 database, these methods are labor-intensive, require extensive preprocessing, and suffer from reduced testing efficiency and model optimization. In recent years, machine learning, notably CNN-based approaches, has emerged as a well-established paradigm in image recognition, streamlining preprocessing and enhancing classification performance [9,10]. Shallow networks, such as CaffeNet and VGG, achieved accuracies ranging from 90.73 % to 95.05 % for five-category classification, while their limited depth constrains their performance in fine-grained fingerprint classification [11,12]. Conversely, deeper networks, such as ResNet, offer greater representational capacity, presenting the potential for more advanced and effective approaches to fingerprint classification [13].

Beyond the first-level primary pattern classification, quantifying more morphometric characteristics offers a more comprehensive understanding of a fingerprint, thereby speeding up recognition processes and revealing population phenotypic heterogeneity. These morphometric attributes include metrics such as fingerprint ridge count (RC), which measures the number of ridges that lie between the core and delta points, and the ridge-valley thickness ratio, among others, as presented in Table 1. These morphometric attributes critically rely on the precise singularity detection in the first phase. Over the past decades, various methodologies have been proposed to detect singularities. For instance, Poincaré Index-based approaches attain a singularity detection accuracy of 97.75 % via closed-loop orientation analysis; however, they are prone to a high false positive rate and poor adaptability to diverse ridge structures [14]. Additionally, manual feature extraction incurs substantial computational burdens and lacks scalability for large datasets. Although deep learning models exhibit progressive improvements in accuracy on singular points detection, such as FCN with 95.39 % accuracy [15], Faster R-CNN with 96.03 % [16], and CP-Net with 96.50 % [17], their functional limitations remain: CP-Net employing multi-level (MLN) and multi-resolution (MRN) networks is confined to core point detection, while the bounding-box paradigm of Faster R-CNN constrains scalability for fine-grained ridge texture measurement. These constraints result in limited subpixel localization precision and hinder robust morphometric analysis. Recent efforts on morphometric

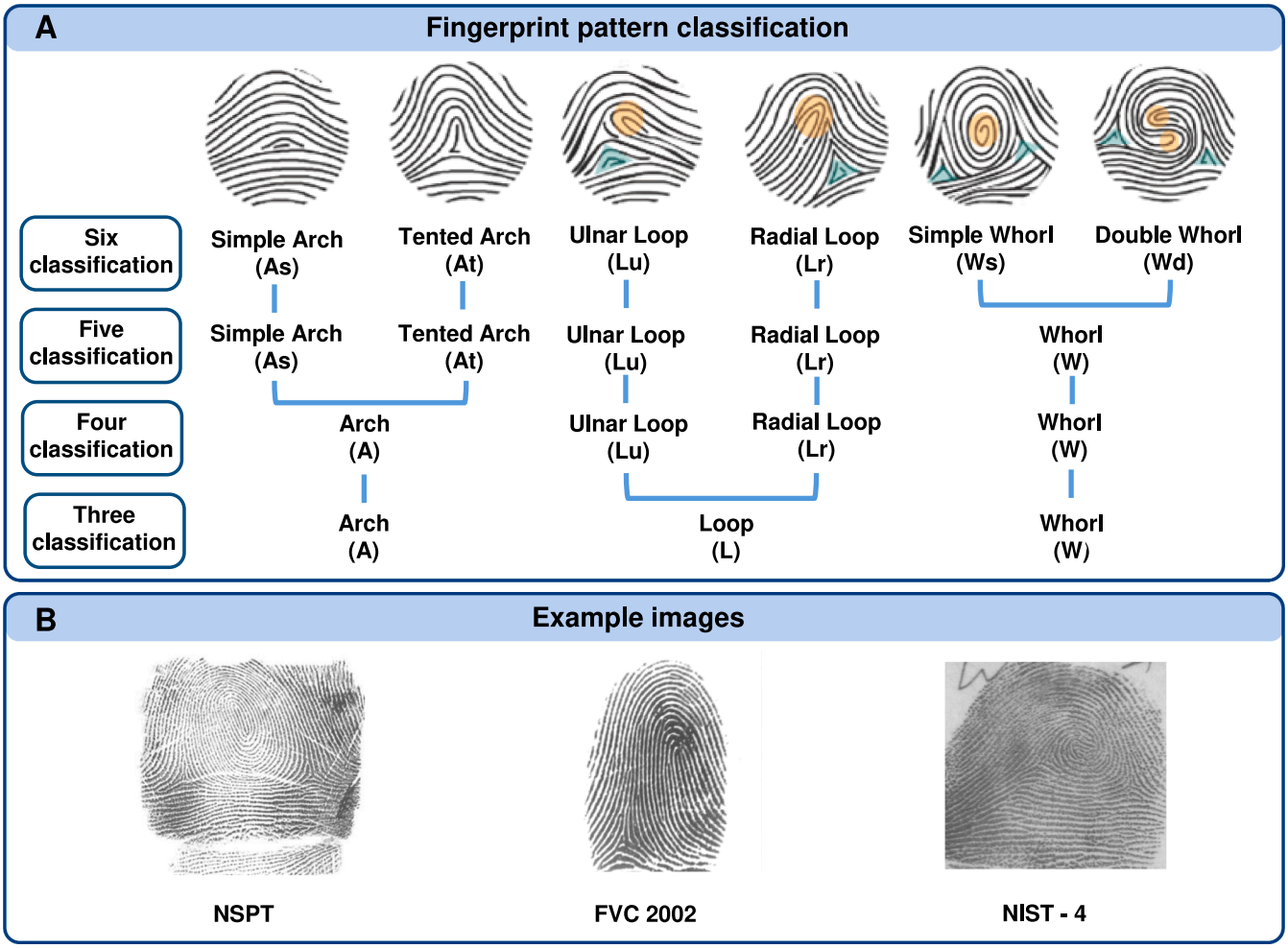

Fig. 1. Illustration of fingerprint pattern classification. (A) Types of fingerprint patterns. Fingerprints can be classified into three major categories: Arch, Loop, and Whorl, based on the presence of deltas, cores, and the direction of ridges. These shapes and contours can be further subdivided into various combinations, such as four classes (without distinguishing between Arch and Whorl), five classes (excluding the separation of Whorl), and six classes. Core and delta points are indicated in orange and green, respectively. (B) Examples of fingerprint images from the private National Survey of Physical Traits (NSPT) dataset, as well as public datasets: Fingerprint Verification Competition 2002 Database 1 (FVC2002 DB1) and NIST Special Database 4 (NIST-4). These include rolled fingerprints, flat fingerprints, and prints obtained by photographing after flat-ink printing, respectively.

Table 1
Morphometric phenotypes of fingerprints (i.e., ridge parameters).

Full Name	Abbreviation	Definition	Schematic Diagram
Ridge count [18]	RC	Measured by counting the intervening ridges between the core and delta of a fingerprint, the ridge count is zero for an arch.	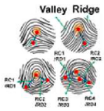
Ridge density [4]	RD	Calculated by dividing the number of ridges counted in a predefined 5 × 5 mm2 area by the area's size.	
Ridge breadth [21]	RB	Defined as the measurement from the center of one furrow across the ridge to the center of the next furrow.	
Mean ridge breadth [21]	MRB	Two measurement techniques for Mean Ridge Breadth (MRB): Mean Individual Ridge Breadth (MIRB) and Mean Ridge - Furrow Pairs Ridge Breadth (MPRB).	/
Mean Individual Ridge Breadth [21]	MIRB	Calculated as the average distance from the center of one furrow, across multiple ridges, to the center of an adjacent furrow.	
Mean Ridge-Furrow Pairs Ridge Breadth [21]	MPRB	Measured by taking prints perpendicularly across multiple ridge breadths simultaneously, then dividing by the number of ridge - furrow pairs	
Ridge thickness [22]	RT	Measured as the width of the high gray level value obtained in the direction normal to ridge flow.	
Valley thickness [22]	VT	Measured as the width of the low gray level value obtained in the direction normal to valley flow.	
Ridge-Valley Thickness Ratio [22]	RVTR	Defined as the ratio of Ridge Thickness (RT) to Valley Thickness (VT).	/
Major angle [6]	MA	Formed by two deltas and the core, the triangle creates the major angle (MA) on either side and defines a perpendicular axis through the core.	
Bisector [23]	Bisector	Angle bisectors of the triangle formed by two deltas and the core intersect. A perpendicular from this intersection to the line joining the deltas determines if it passes through the core or deviates right or left.	

phenotypes quantification achieves 96.6 % exact-match accuracy and 1.1 % EER on FVC2002 plain fingerprints [18], but generalize poorly to rolled or cross-sensor fingerprint data and support only short-range ridge counts (< 15), which are inadequate for capturing full core-to-delta spans required in many biomedical applications. Consequently, a critical gap remains in the absence of an end-to-end, scalable framework capable of high-accuracy multi-dimensional morphometric quantification.

This paper proposes an integrated deep learning framework, FPQuant, for the precise quantification of 12 fingerprint phenotypes. The framework, built on deep neural networks, first classifies fingerprint patterns and then uses the CSPNeXt backbone network to detect singular points with high precision, converting the task into a subpixel classification of horizontal and vertical coordinates [19]. Furthermore, a Depth-First Search (DFS)-based connected component detection algorithm is incorporated to accurately quantify morphometric features such as ridge count and ridge density. FPQuant is applied to quantify fingerprint phenotypes in 28,867 fingerprint images from 3078 Han Chinese individuals, revealing significant population heterogeneity across six phenotypes. This advancement enhances the efficiency of biometric applications for identity verification using large-scale fingerprint databases and provides a scalable infrastructure for biological anthropology, population genetics, and medical research.

2. Material and methods

2.1. Model-construction datasets

In the model-construction phase, this study utilizes a self-built Chinese fingerprint dataset from the National Survey of Physical Traits (NSPT), a subject of The National Science & Technology Basic Research Project. The dataset comprises cross-sectional fingerprint images collected from three geographically distinct regions of China, from north to south: Zhengzhou (NSPT-ZZ, n = 10,246), Taizhou (NSPT-TZ, n = 4937), and Nanning (NSPT-NN, n = 13,684), with all images captured using standardized DactyScan40i rolled fingerprint scanner at 800×750 pixel resolution. Each fingerprint image contains four annotation layers (six-, five-, four- and three-class taxonomies; Fig. 1A), independently labeled by two trained dermatoglyphics experts and subsequently verified by a third expert, with all decisions documented to ensure annotation reliability and reproducibility. This established consensus-based protocol was also applied to ensure the consistency of ridge counting in 50 samples, as detailed in Section 4.3. A subsample of 1000 NSPT-ZZ images underwent additional annotation for precise coordinate mapping of singular points using Labelme software [20], thereby to estimate morphometric phenotypes of fingerprints (Table 1). For neural network optimization, we implemented a stratified sampling strategy allocating 6976 NSPT-ZZ samples to training/validation (7:3 split), while reserving the remaining 21,891 samples (comprising NSPT-NN, NSPT-TZ, and the remaining NSPT-ZZ samples) for comprehensive algorithm validation through cross-regional testing.

2.2. Cross-validation datasets

To rigorously assess algorithm generalization, we established a dual verification protocol using benchmark fingerprint databases: a) fingerprint classification validation: the NIST Special Database 4 (NIST-4; n = 4000) [24] with five-class taxonomy (arch, left loop, right loop, tented arch and whorl) served as the primary benchmark. This database maintains strict class balance through dual-label assignments, where ambiguous patterns receive complementary classifications. Following contemporary computational fingerprinting practices, we prioritized primary labels during model training while accepting either annotated class as valid during performance evaluation; b) singular point detection validation: the Fingerprint Verification Competition 2002 Database 1 (FVC2002 DB1; n = 800) [25], containing annotated singular points in flat impressions, provided validation for singularities region detection. This stratified validation architecture explicitly separates classification accuracy assessment from feature detection robustness evaluation. The implementation details of cross-database validation protocols and corresponding data distribution are systematically outlined in Table 2.

3. Proposed architecture

The proposed model architecture consists of three distinct modules: the Fingerprint Pattern Classification Module (FPCM), the Singularity

Table 2
Distribution of fingerprint patterns in different datasets.

Datasets		Sample size	Image size (pixel)	Experiment scheme (% of total samples)	As	At	Lu	Lr	Ws	Wd	Singular points
Our datasets	NSPT-ZZ	10,246	800×750	Train: Val = 60 %: 10 % Test (30 %)	88 23	55 26	1788 822	1810 794	2896 1426	339 179	800 200
	NSPT-TZ	4937	800×750	Test (100 %)	79	40	1344	1353	1812	309	/
	NSPT-NN	13,684	800×750	Test (100 %)	297	48	3748	3770	5072	749	/
Public datasets	NIST-4	4000	512×512	Train: Val = 37.5 %:12.5 % Test (50 %)	394 406	388 412	221 579	603 197	394 406		/
	FVC2002 DB1A	800	388×374	Test (100 %)	/	/	/	/	/	/	800

Point Detection Module (SPDM), and the Morphometric Phenotype Quantification Module (MPQM) (Fig. 2). The FPCM employs a ResNet18 deep residual neural network as a feature extractor to perform a multi-class classification of fingerprint pattern modalities, enabling the quantification of fingerprint phenotypes. The output of the FPCM, which represents the fingerprint pattern modality class, serves as an adjustable threshold input for the SPDM. The SPDM uses CSPNeXt [26] as its backbone network for feature extraction and transforms the coordinate prediction task into a sub-pixel classification problem, thus enhancing the accuracy of singularity point detection [27]. Finally, the MPQM module takes the singular point detection results from the SPDM as input and applies a DFS-based connected components detection algorithm to automate the quantification of fingerprint morphometric phenotypes. The system, given an input fingerprint scan image, is capable of generating at least 12 distinct fingerprint phenotypes in a unified and efficient process.

3.1. Fingerprint pattern classification module (FPCM)

This paper proposes a deep learning classification framework using residual convolutional neural networks, in contrast to traditional fingerprint classification methods based on handcrafted features. This framework enables the automatic, joint learning of discriminative features and fingerprint classification from the original images. To hierarchically learn the features of fingerprint images for classification, the ResNet18 network was employed (Figure S1), with its architecture and parameters detailed in Fig. 2.

A novel loss function is introduced to address class imbalance among fingerprint categories. By assigning higher weights to minority classes (i.e., those with fewer samples), the model's performance in recognizing these classes is improved. The following focal-loss function is employed for fingerprint image classification:

$$FL = \frac{1}{N}\sum_{i} L_i = -\frac{1}{N}\sum_{i=1}^{M}\sum_{c=1} y_{ic}\alpha_c(1-p_{ic})^{\gamma}\log(p_{ic}) \quad (1)$$

where N was the number of samples, M was the number of classes, p_{ic} was the predicted probability that the observed sample i belongs to the category c, and y_{ic} was the ground truth. If the real class of sample i was equal to c, y_{ic} was equal to 1; otherwise, it equaled to 0, $\alpha_c$represents the weight for class c, defined as: $\alpha_c = \frac{N}{M\times n_i}$, where n_i is the number of samples in class i. The modulation factor γ was set to the empirical value of 2 in the experiments [28].

In training the proposed network, the learning rate is initialized set to 1×10^{-3} for all layers and is reduced by a factor of 10 when the loss plateaus after 5 epochs. The Adam optimizer, with momentum set to 0.9 and weight decay set to 1×10^{-4}, is used. The network is trained for 100 epochs, and the best model is selected based on performance on the validation set.

Additionally, the fingerprint classification is sensitive to image rotation. Most of existing methods computed the image rotation for fingerprint alignment, followed by classification. Instead of directly computing image rotation, random rotations between −10 and 10 degrees are applied as data augmentation during training to enhance the model's robustness to rotational variations.

3.2. Singular point detection module (SPDM)

This section proposes a Fingerprint Singular Point Detection (FingerSPD) algorithm, which utilizes CSPNeXt [8] as the backbone network for feature extraction due to the complexity of fingerprint images. CSPNeXt integrates Cross-Stage Partial (CSP) feature fusion with NextNet's grouped convolutions and channel-wise attention mechanisms [26]. This design enables the network to focus on regions around singularities, enhancing the representation of key features. Grouped convolutions optimize feature extraction and computational efficiency while maintaining a lightweight structure that reduces memory usage and inference time.

Traditional keypoint detection methods often frame the problem as regression or heatmap-based classification, which can lead to lower accuracy, high computational cost, and complex post-processing. To address these issues, we discretize the continuous coordinate values by dividing the horizontal and vertical axes into equally spaced bins, transforming keypoint localization into a classification task. The model is trained to predict the bin containing the keypoint. By increasing the number of bins, we reduce quantization error to a sub-pixel level, thus improving localization accuracy [27]. In this module, we employ 1×1 convolutional layers to convert the features extracted by the backbone network into a vectorized representation of keypoints, followed by two fully connected layers for classification. This results in a streamlined algorithm structure.

In the coordinate encoding phase, the x and y coordinates of the keypoints are represented as two independent one-dimensional vectors, with the length of each vector determined by a scaling factor λ (≥ 1). For the k-th keypoint, the encoded coordinates are represented as follows:

$$k' = (x', y') = \left(round\left(x^k * \lambda\right), round\left(y^k * \lambda\right)\right) \quad (2)$$

The scaling factor λ refines the localization accuracy to a level finer than a single pixel, and the value is adaptively determined by the input image. Its value needs to be determined based on the actual image conditions. In the decoding phase, the model outputs two one-dimensional vectors. The predicted coordinates of the keypoint are computed as:

$$\widehat{o}_x = argmax_i(o_x(i)) \;/\; \lambda, \widehat{o}_y = argmax_j\left(o_y(j)\right) \;/\; \lambda \quad (3)$$

Thus, the position of the maximum value along each one-dimensional vector is divided by the scaling factor λ to revert to the image scale. Finally, the two decoded values are concatenated to obtain the keypoint's position.

The experimental setup utilizes two NVIDIA RTX 3090 graphics

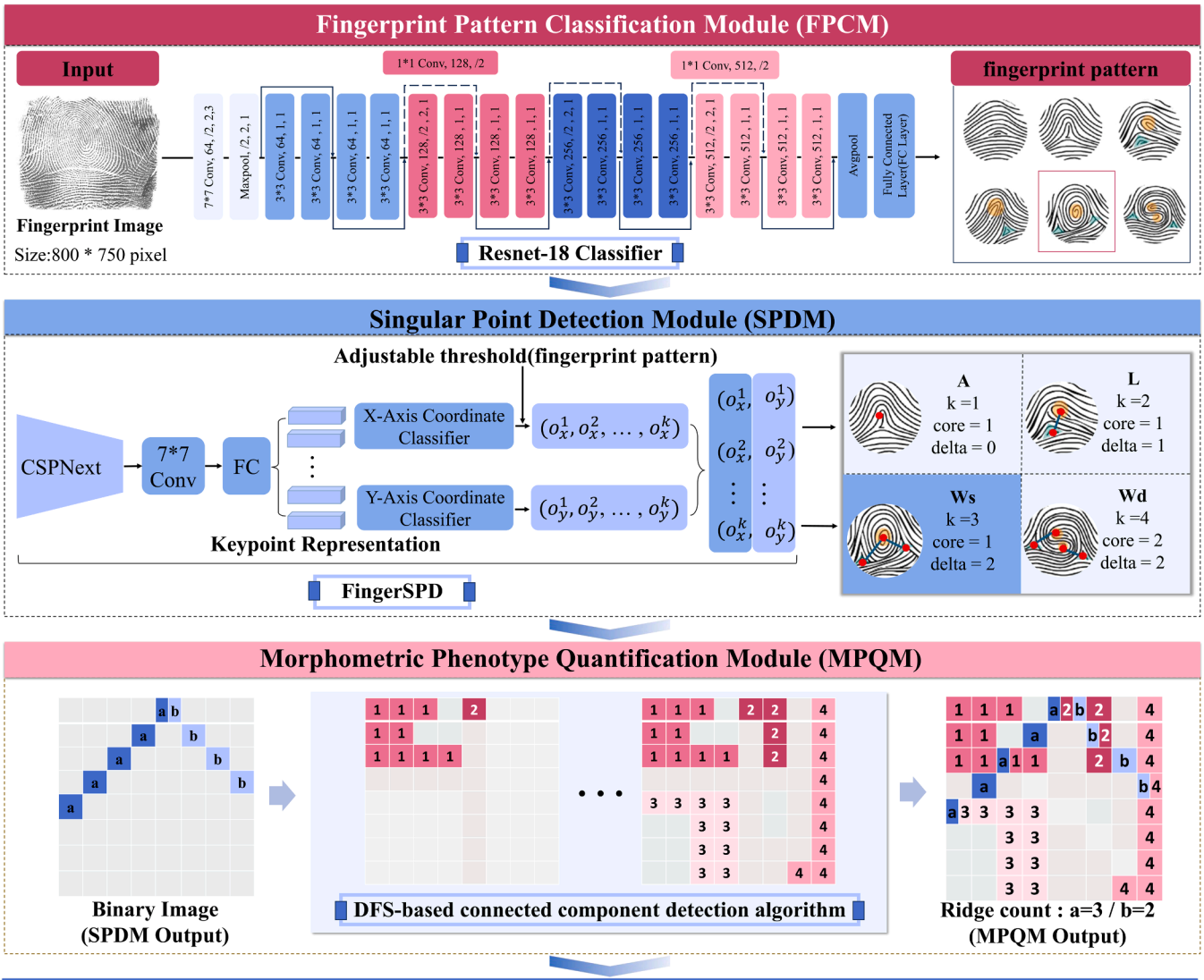

Output

Fingerprint phenotypes		Number of traits	Value
Classified phenotypes	Pattern	1	Ws
Morphometric phenotypes	Ridge breadth(RB) / *mm*	x	/
	Ridge thickness(RT) / *mm*	x	/
	Valley thickness(VT) / *mm*	x	/
	Ridge-valley Thickness Ratio(RVTR)	x	/
	Ridge density(RD)	2	Left:9.14 Right:8.55
	Mean individual ridge breadth(MIRB)	x	/
	Ridge counts(RC)	2	Left:15.00 Right:11.00
	Mean ridge-furrow pairs ridge breadth(MPRB) / *mm*	2	Left:0.77 Right:0.82
	Distance between core and delta / *mm*	2	Left:11.60 Right:9.10
	Major angle(MA) / °	2	Left:49.56 Right:45.23
	Bisector	1	Left

Fig. 2. General framework of fingerprint phenomics quantification.

cards, equipped with CUDA v11.2 for efficient GPU-accelerated computing. The deep learning framework employed is PyTorch v1.10. During training, a batch size of 8 is used to balance computational efficiency and memory consumption. The model is trained for a maximum of 250 epochs to ensure the learning of relevant features. The initial learning rate is set to $1 \times 10^{-3,}$ which is dynamically adjusted throughout training to improve convergence speed and stability. Additionally, input images are resized to 800×750 pixels, with necessary scaling and cropping operations performed during preprocessing.

Several evaluation metrics are employed to assess the performance of

the fingerprint singularity detection algorithm:

- AP (Average Precision): This metric measures the average prediction accuracy across multiple categories, with a higher AP indicating better prediction performance. It is calculated as:

$$AP = \int_{1}^{0} Precision(Recall)d(Recall) \tag{4}$$

- TDR (True Detection Rate): A predicted point is considered correct if it falls within a circle with a radius of k pixels centered on the true location. The predicted location is considered a true core point if it lies within k pixels of the actual location. The formula for this is:

$$\sqrt{(C_p x - C_a x)^2 + (C_p y - C_a y)^2} \leq k \ pixels \tag{5}$$

Where C_p and C_a refer to predicted and ground truth coordinates, respectively. In this study, the evaluation radius was set to 20 pixels. This value was determined based on the average ridge width in our 600 dpi NSPT dataset (Figure S2), ensuring that the evaluation area does not extend beyond a single ridge. This setting is also consistent

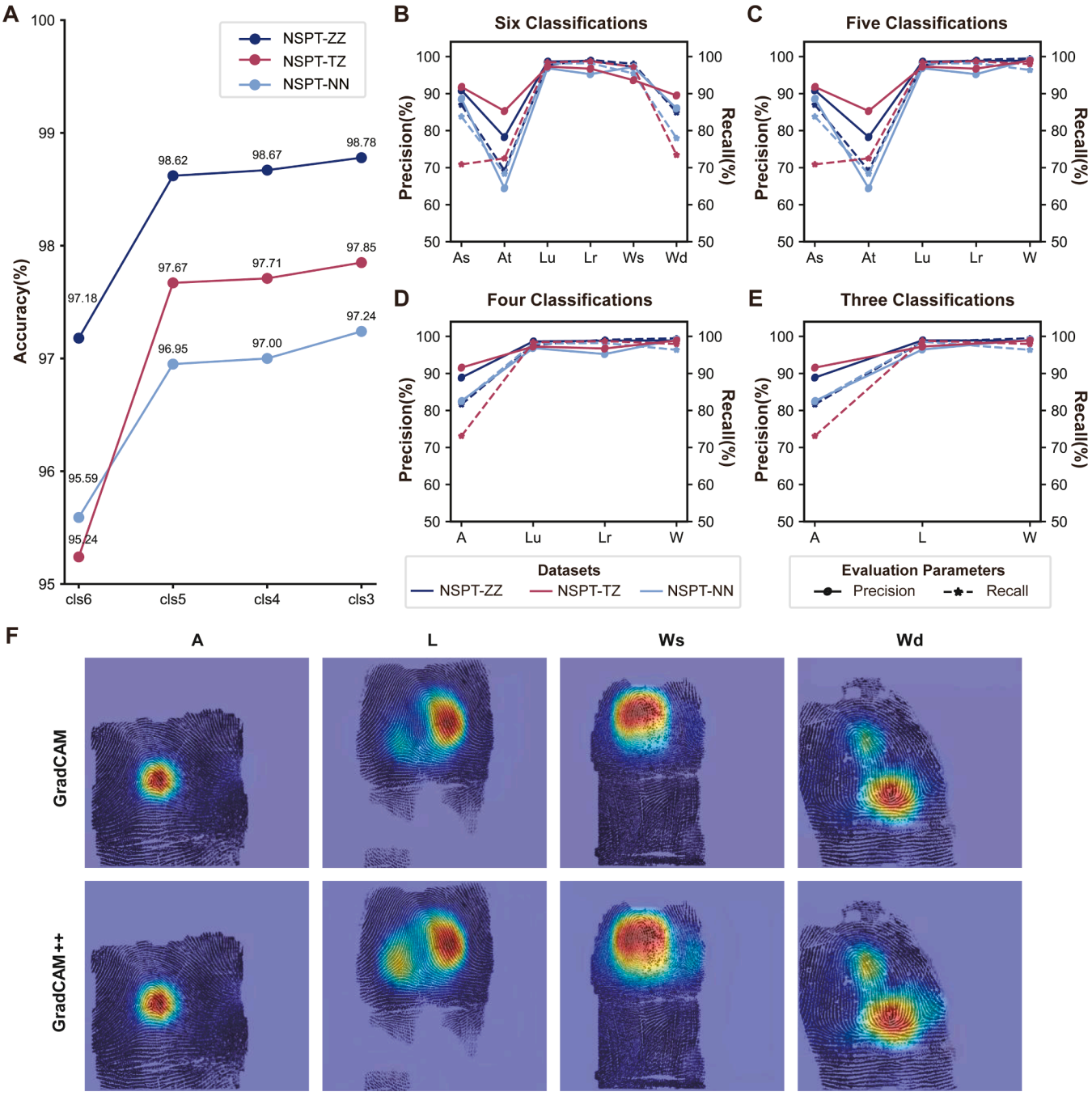

Fig. 3. Performance and visual feature attribution of the fingerprint pattern classification module (FPCM). (A)-(E) The accuracy, precision and recall rates of six-class, five-class, four-class, and three-class classification tasks in the NSPT databases. The classification criteria are detailed in Fig. 1A. (F) Salient fingerprint features identified by the network using Grad-CAM (top) and Grad-CAM++ (bottom) for pattern classes A, L, Ws and Wd. Warmer colors indicate greater contribution to classification.

with the parameter used in a prior benchmark study [17].

3.3. Morphometric phenotypes quantification module (MPQM)

The quantification of morphometric phenotypes in fingerprints initiates with the computation of the ridge count (Table 1). This process begins by initializing a labeled image along with a statistical information array. We then traverse each pixel, commencing from the top-left corner of the image, to determine if connected component analysis is required based on the pixel's labeling status and value. For unlabeled pixels indicating a foreground (i.e., representing a ridge), we initiate a new connected region and assign a distinct label. Utilizing the Depth-First Search (DFS) algorithm, we label all connected foreground pixels within that region while concurrently computing and storing statistical information along with the centroid coordinates. Labeled pixels or those representing the background (i.e., exhibiting values indicative of non-ridges) are excluded from this analysis. Upon completion of the pixel traversal, we compile the total number of connected regions, the labeled image, the statistical information array, and the centroid coordinates array, which are critical for the subsequent calculations of additional morphometric fingerprint phenotypes.

The statistical analysis in this study was conducted using ANCOVA. Initially, normality and homogeneity of variance tests were performed on the dataset, followed by covariance analysis. A model was established with RD and MPRB as the dependent variables, group as the independent variable, and Sex and Age as covariates. The analysis was carried out using the statsmodels package in Python.

4. Experiments and results

4.1. Fingerprint pattern classification

To assess the performance Resnet-18 in fingerprint pattern classification module (FPCM), we evaluated the accuracy, precision and recall metrics across four testing datasets from various fingerprint databases. On three self-constructed test sets for 6-class classification, the FPCM achieved accuracies of 97.18 %, 95.59 %, and 95.24 %, respectively. In the five-, four- and three-class classification scenarios, the accuracy rates gradually improved, and the NSPT-ZZ dataset, which was the data source for model training, exhibited the highest accuracy at 98.78 %. The accuracies rates of the other two datasets also remained at above 97.24 %, highlighting the generalizability of the proposed algorithm across different distributions without the need for transfer learning (Fig. 3A). Further analysis of precision and recall rates of each subclass revealed that, compared with other categories, the simple arch (As), tented arch (At), and double whorl (Wd) types with lower prevalence exhibited lower precision and recall rates (Fig. 3B-E), which could be attributed to the various class imbalances in the dataset (Table 2). Comprehensive confusion matrices for all datasets and tasks are provided in Supplementary Data. Importantly, visual explanations from Grad-CAM/Grad-CAM++ (Fig. 3F) demonstrate that the model's decisions are grounded in well-established fingerprint structures (core, delta regions and ridge direction flow)—anatomically meaningful areas critical for fingerprint classification—thereby validating the biological plausibility of the learned features.

The NIST-4 database, a standard reference in fingerprint image analysis, features non-rolling scanned image types and balanced distribution of five-class fingerprint patterns, which is different from the samples used to construct model in this study (Fig. 1B, Table 2). Initial direct evaluation of FPCM algorithm on NIST-4 yielded 83.70 % classification accuracy (Table 3), revealing domain shift limitations. Therefore, we implemented a transfer learning framework with partial domain adaptation, fine-tuning the pre-trained deep network of FPCM on 50 % of the NIST-4 database samples. This strategic retraining achieved the highest five-class classification accuracy of 96.20 %, outperforming existing methods (Table 3), demonstrating the effectiveness of the proposed algorithm in leveraging multi-level features to achieve superior classification performance.

Table 3
The accuracy of five-class pattern classification in NIST-4 reference database.

Studies	Method	Training	Test	Accuracy of five-classes (%)
Zhang and Yan [29]	Singularity -based	/	NIST-4	84.30
Yao et al. [30]	Structure-based	/	NIST-4	89.30
Tan et al. [31]	Structure-based	/	NIST-4	91.60
Daniel et al. [32]	CNN: CaffeNet	SfinGedatabases (n = 10,000), NIST-4 (n = 1650)	NIST-4 (n = 2350)	90.73
Michelsanti et al. [11]	CNN:VGG-F	NIST-4 (n = 3900)	NIST-4 (n = 100)	94.40
Michelsanti et al. [11]	CNN:VGG-S	NIST-4 (n = 3900)	NIST-4 (n = 100)	95.05
Akhila et al. [12]	Lightweight CNN	NIST-4 (n = 3600)	NIST-4 (n = 400)	93.75
Proposed	Resnet-18 Classifier	NSPT-ZZ (n = 6976)	NIST-4 (n = 4000)	54.05(without preprocess)
		NSPT-ZZ (n = 6976)	NIST-4 (n = 4000)	83.70
		NSPT-ZZ (n = 6976), NIST-4 (n = 2000)	NIST-4 (n = 2000)	96.20

4.2. Fingerprint singular point detection

This section employed a triple-metric evaluation framework encompassing average precision (AP), true detection rate (TDR) and cross-dataset benchmarking to assess the phenotyping capabilities of the proposed FingerSPD algorithm in Singular Points Detection Module (SPDM). At epoch 200, the training loss value tended to be stable at 0.01 and the validation Average Prevision (AP) at 98.63 %, indicating robust convergence of the model (Fig. 4A). The TDR values of the four fingerprint patterns (i.e., arch, loop, simple whorl, and double whorl) were all greater than 98.00 %, highlighting the robust generalization performance of the FingerSPD algorithm in singularity point detection (Fig. 4B).

Notably, our proposed FingerSPD incorporates a discretization factor λ to regulate the number of bins per pixel in its sub-pixel classification stage, with $\lambda = 2$ determined as optimal for balancing precision and complexity (Section 3.2; Fig. 4C). Unlike Faster R-CNN, FingerSPD's subpixel singularity detection eliminates the need for complex anchor-based computation or post-processing steps such as non-maximum suppression, which substantially improves localization accuracy, yielding a subpixel error of <0.5 px.

To interpret the learned representations, we visualized activations from the final convolutional layer via heatmapping, which served as a tool for assessing the model's interpretability and rationality of its learned representations. The resulting attention maps reveal that the model, guided by CSPNeXt's channel-attention mechanism, selectively focuses on ridge textures while avoiding redundant feature extraction. Notably, activations are predominantly concentrated around singular points (Fig. 4D), confirming that the network leverages structurally meaningful regions for decision-making.

The proposed FingerSPD achieved an impressive 97.75 % TDR on the public database FVC2002 DB1, demonstrating its competitiveness with existing methods (Table 4). Furthermore, by integrating the prior knowledge from the FPCM results, our method not only enables

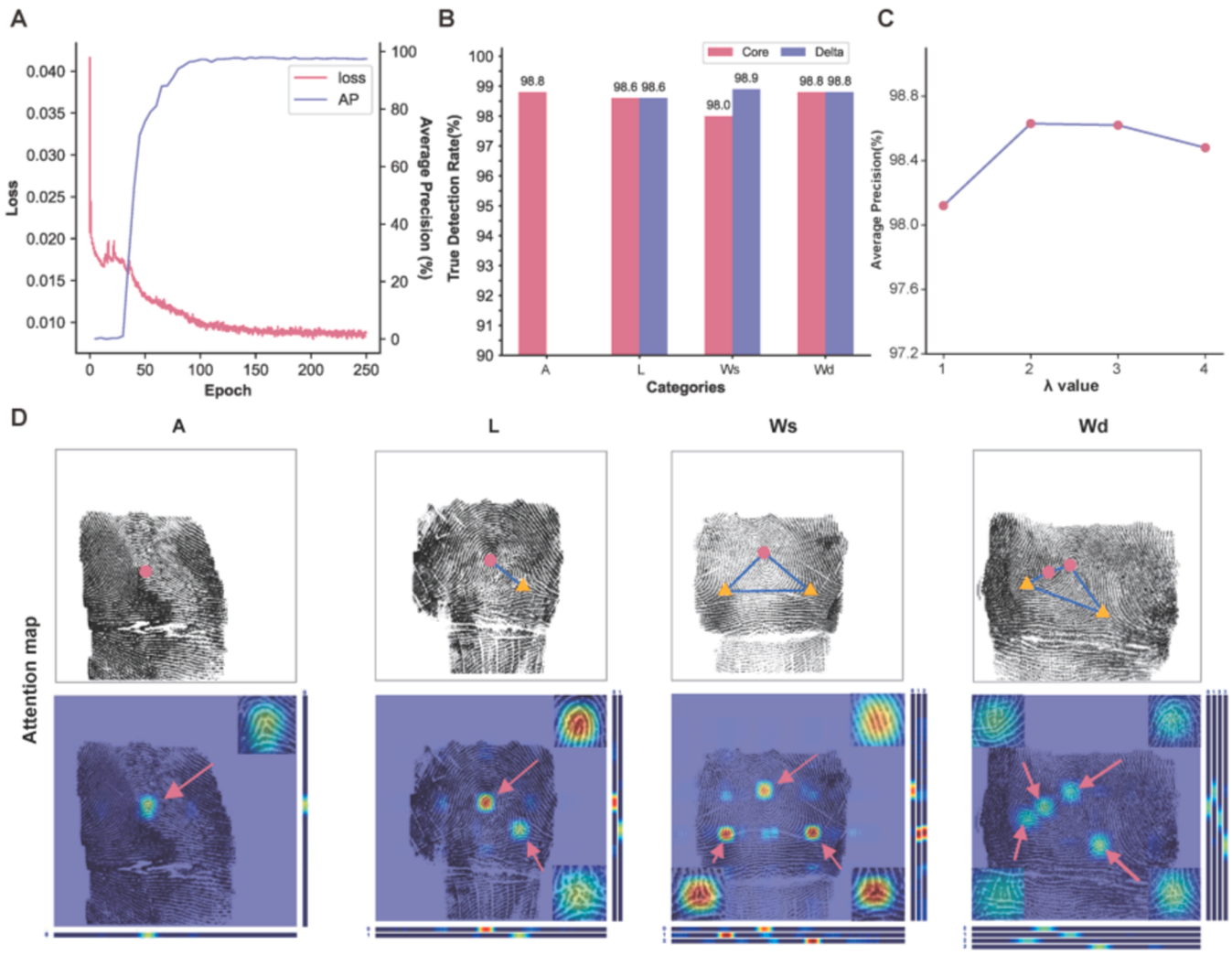

Fig. 4. The singularity detection precision in NSPT databases. (A) Model performance during the training process, illustrating the changes in the loss function for the training set in relation to the training steps, and the variations in Average Precision (AP) for the validation set. (B) The True Detection Rate (TDR) of the model on the validation set from the self-constructed Chinese database. The Arch patterns do not contain delta singularity. (C) Ablation study of the discretization factor λ in FingerSPD. λ controls the number of bins per pixel in sub-pixel classification. Model performance increases initially and then decreases as λ grows, with an optimal value at $\lambda = 2$. (D) Visualization of FingerSPD's fingerprint singularity detection region.

Table 4
Performance of fingerprint singularity detection of different algorithms.

Studies	Methods	Training set	Test set	Output on FVC2002 dataset			
				Core		Delta	
				TDR (%)	FAR (%)	TDR (%)	FAR (%)
Zhou et al. [33]	Differences of the ORlentation	/	FVC2002 DB1 ($n = 800$)	95.78	2.27	96.98	9.97
Qin et al. [15]	Fully Convolutional Networks	Private dataset ($n = 15{,}000$)	FVC2002 DB1 ($n = 800$)	95.39	1.03	98.26	4.10
Liu et al. [16]	Faster R-CNN	FVC2002 ($n = 400$), NIST sd04 ($n = 2000$), Ten-Finger Card ($n = 50{,}124$)	FVC2002 DB1 ($n = 400$)	96.03	0.92	98.33	3.88
G. Arora et al. [17]	CP-Net (MLN and MRN)	FVC2002 ($n = 600$), FVC2004 ($n = 600$), FVC2006 ($n = 1260$)	FVC2002 DB1 ($n = 200$)	96.50	0	/	/
Proposed	FingerSPD	NSPT-ZZ ($n = 800$), FVC2002 ($n = 400$)	FVC2002 DB1 ($n = 400$)	97.75	0	95.00	0
			NSPT-ZZ ($n = 200$)	98.50	0	98.79	0

simultaneous detection of core and delta points but also eliminates the false acceptance rate (FAR) entirely. This significant enhancement expands the potential applications of our approach in fingerprint recognition.

4.3. Fingerprint morphometric phenotypes quantification

The Morphometric Phenotype Quantification Module (MPQM) implemented a rigorous evaluation framework to assess the reliability of our Depth-First Search (DFS)-based connected components detection algorithm for ridge counting between singularities. A triple-blind comparative analysis involving three experts (denoted as M) and the algorithmic system (denoted as P) was performed on 50 representative samples. Statistical analysis revealed no significant inter-rater discrepancies among experts ($p = 0.50$; Intraclass Correlation Coefficient, ICC = 0.95) nor differences between experts (P) and computational evaluation (M) ($p = 0.72$; ICC = 0.94) in ridge count quantification (Fig. 5A). Notably, 46 % of samples (23/50) demonstrated perfect concordance in error patterns between manual and automated counts, exceeding the incidence of larger (24 %; 12/50) or smaller (30 %; 15/50) discrepancies in human annotations (Fig. 5B). The maximum observed deviation between modalities was constrained to 3 ridge lines (Mean Absolute Difference: MAD = 1.24), establishing operational feasibility for population-level analyses. The framework could also be extended to ridge density, breadth, and thickness quantification with sub-pixel precision (Table 1).

The proposed unified deep learning framework achieves enhanced computational efficiency compared to traditional methods that rely on rules, handcrafted features, or isolated models. Although the training of the network may demand more time, the testing process with the trained model is remarkably swift. As shown in Table 5, the framework demonstrates order-of-magnitude improvements across all processing stages compared to conventional approaches. Specifically, the FPCM on pattern classification executes in 6.30 ms, which is 10 times faster than rule-based (100.20 ms) and handcrafted-features (39.00 ms) approaches. The SPDM on singular point detection achieves 95.00 ms, surpassing CP-Net (165.00 ms) and BC (253.00 ms). The MPQM on quantification takes just 10.40 ms per image. The proposed framework integrating FPCM, SPDM, and MPQM, takes 118.00 ms per image, making it ideally suited for rapid and accurate fingerprint analysis in real-time and large-scale tasks.

Table 5
Time consuming comparison.

Modules	Methods	Hardware Configuration	Time Consumption (ms)
FPCM	CNN: CaffeNet [32]	NVIDIA GTX TITAN GPU	100.20
	CNN: VGG-F [11]	NVIDIA GTX 950 M GPU	39.00
	CNN: VGG-S [11]	NVIDIA GTX 950 M GPU	77.00
	Proposed	NVIDIA GTX 3090	6.30
SPDM	CP - Net [17]	NVIDIA GTX 1080 Ti	165.00
	Proposed	NVIDIA GTX 3090	95.00
MPQM	Proposed	NVIDIA GTX 3090	10.40
End - to - end of the proposed framework	Proposed	NVIDIA GTX 3090	118.00

4.4. Population-specific fingerprint profiling using multi-dimensional phenotypes

Employing the FPQuant computational framework, we conducted systematic biometric profiling of Han Chinese populations across three geographically distinct cohorts from north to south of China (NSPT-ZZ: $n = 1039$; NSPT-TZ: $n = 521$; NSPT-NN: $n = 1518$ participants). The framework's multivariate analysis pipeline simultaneously quantifies phenotypic parameters, such as Pattern classification, Ridge Count (RC), Ridge Density (RD), Mean Ridge-Furrow Pairs Ridge Breadth (MPRB), Major angle (MA), and Bisector (Table 1).

Cross-population analysis revealed significant biogeographic divergence in fingerprint characteristics (Fig. 6; Table S1). Specifically, substantial inter-regional differences emerged in whorl patterns, with NSPT-ZZ demonstrating elevated prevalence of simple whorls (Ws: 42.18 % vs. NSPT-NN 37.07 %, $p = 4.00\times10^{-12}$; vs. NSPT-TZ 36.7 %, $p = 2.62\times10^{-16}$), while NSPT-NN exhibited unique simple arch predominance (As: 2.17 % vs. other regions, $p = 1.36\times10^{-15}$). In addition, highly bilateral symmetry in digits with the same name (left-right consistency > 0.05, Figure. S3) contrasted with marked digit-specific

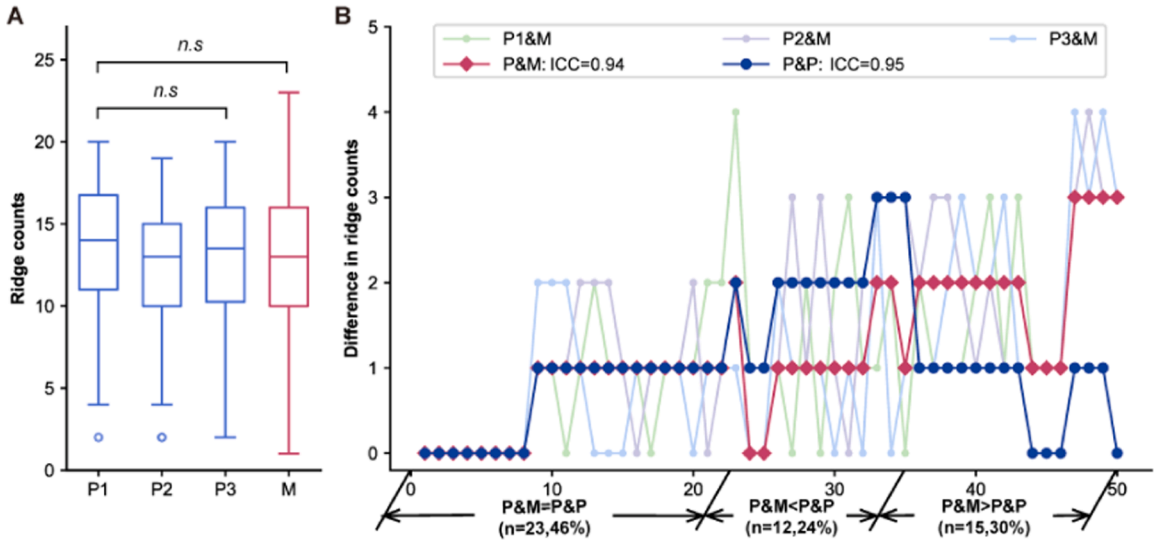

Fig. 5. The measurement of ridge counts in 50 fingerprints of NSPT dataset. **(A)** Box plot comparison of ridge count results between the three experts-level (P) and algorithm-based (M) model. The differences between groups were analyzed by Analysis of Variance (ANOVA); **(B)** Visualization of ridge count errors between the machine and expert counts across 50 test images. P1-P3 represent the ridge count results of the three experts, P&P denotes the average ridge count error among the three experts, and P&M indicates the average ridge count error between the model and the three experts.

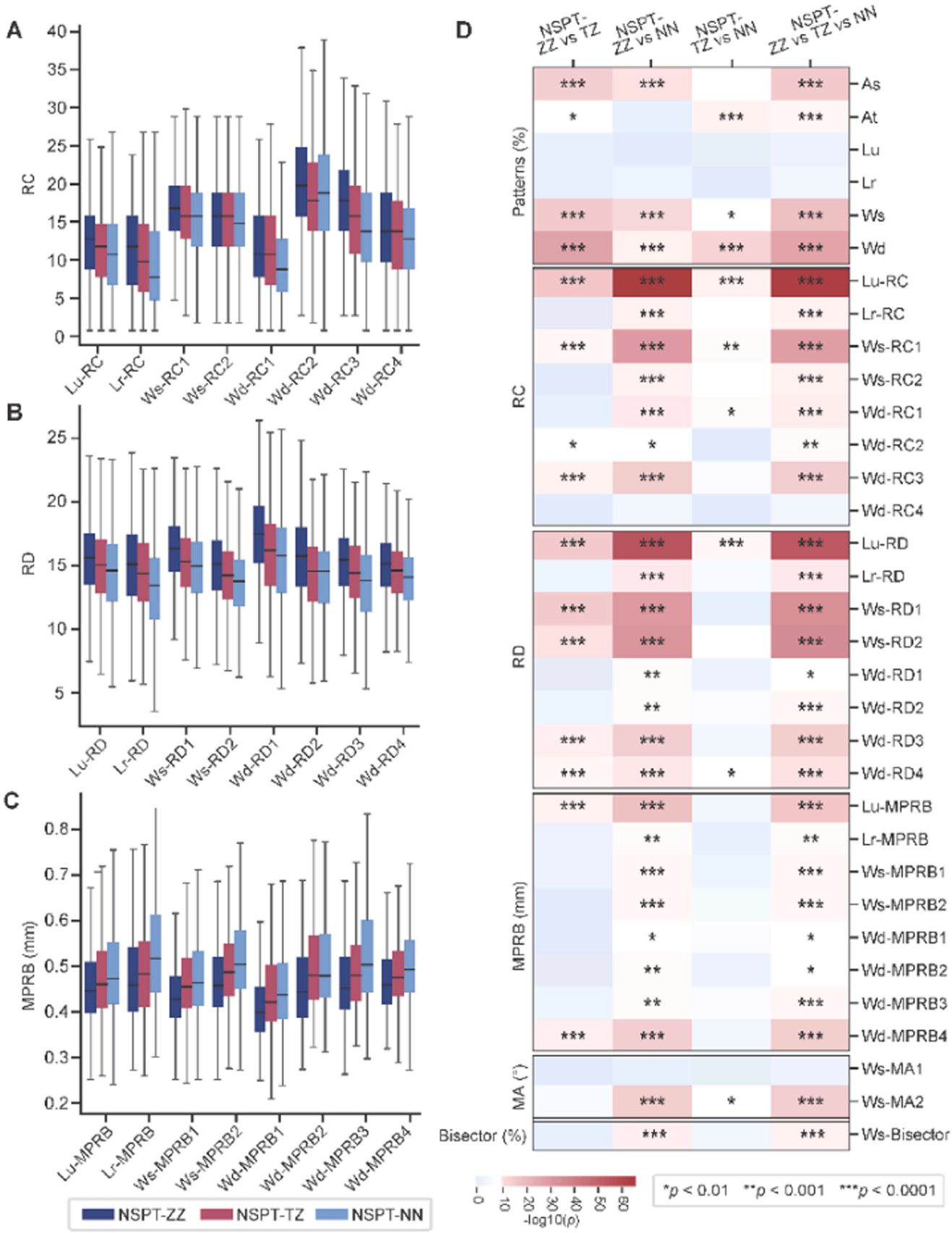

Fig. 6. Comparison of fingerprint morphometric phenotypes across three NSPT datasets. **(A)** Ridge count (RC), **(B)** Ridge density (RD), **(C)** Mean ridge-furrow pair ridge breadth (MPRB) distributions shown as box plots. Blue, red, and gray indicate NSPT-ZZ, NSPT-TZ, and NSPT-NN, respectively. **(D)** Heatmap showing pairwise population differences for fingerprint pattern types, RC, RD, MPRB, and major angle (MA) phenotypes. Color scale represents -log(p) values; asterisks denote statistical significance (*$p < 0.01$, **$p < 0.001$, ***$p < 0.0001$).

patterning, e.g., the Ws pattern dominated on ring fingers (29.95 %), Lr prevailed on the index finger (74.31 %), and Lu was predominant on the middle finger and little fingers (79.55 %, Figure. S4).

Quantitative analyses of morphometric characteristics uncovered unreported biogeographic variation of fingerprints cross populations. NSPT-ZZ - NSPT-NN comparisons revealed obvious ridge count (RC) divergence in ulnar loop patterns ($\Delta RC = 1.59$; $p = 1.88\times10^{-65}$ - 9.54×10^{-17}). The ridge density (RD) was the highest in NSPT-ZZ with decreasing among three populations from north to south (NSPT-ZZ 15.34 > NSPT-TZ 14.62 > NSPT-NN 14.23; $p = 3.50\times10^{-25}$), while MPRB showed the increased regional trends (NSPT-ZZ: 0.51 < NSPT-TZ: 0.55 < NSPT-NN: 0.57; $p = 2.75\times10^{-9}$). Notably, significant differences were observed in the MA ($\Delta MA = 1.8^{\circ}$; $p = 1.18\times10^{-14}$) and Bisector positional offsets ($p = 2.05\times10^{-6}$), exposing previously undocumented whorl imbalance gradients in large-scale population study.

5. Discussion

This study proposes FPQuant, a unified and automated framework for fingerprint phenotyping that integrates three core modules: fingerprint pattern classification (FPCM), the singular point detection (SPDM), and the morphometric phenotype quantification (MPQM). By leveraging a data-driven manner, the framework takes fingerprint images as input and outputs corresponding fingerprint phenotypes, including fingerprint patterns and eleven morphometric phenotypes. It demonstrates excellent accuracy, generalization performance and integration capability, marking substantial advancements in multiple quantification of fingerprint phenotypes. Its strong performance and scalability have enabled the first large-scale analysis of fingerprint morphometric heterogeneity in a Han Chinese cohort. These quantitative traits may reflect underlying genetic regulation, as evidenced by prior genome-wide association studies (GWAS) and developmental studies implicating WNT, EDAR, and BMP signaling pathways in ridge patterning, spacing and size [2, 34]. These findings reinforce the potential of FPQuant as a powerful tool for bridging morphological fingerprints with genetic underpinnings and facilitating future biomarker discovery.

The principal methodological innovation of FPQuant lies in its subpixel-level singularity detection capability. The dedicated FingerSPD module achieves precise singularity localization at the subpixel level without relying on anchor-based detection or additional post-processing steps, by reformulating the task as two independent classification problems for horizontal and vertical coordinates and uniformly dividing each pixel into multiple bins [27]. This approach not only ensures high localization accuracy (with a mean error of <0.5 pixels) but also reduces computational overhead.

A specific challenge in ridge counting measurement lies in ridge thinning [35], a necessary step for obtaining direction information but potentially leading to ridge deformations, such as cuts, twigs or cross ridges absent in original images. To address this issue, we implemented a DFS-based connected component detection algorithm, which effectively identifies and groups connected pixels in the image, thereby enhancing the precision of ridge representation. However, errors in detecting strongly connected components may occur if ridges touch due to unclear images or uneven pressure during acquisition (Fig. 7C).

Three main limitations should be noted. First, data generalizability and reproducibility: The model was trained predominantly on a Han Chinese cohort, which may limit its generalizability to other populations with distinct morphometric traits. Furthermore, the use of a private dataset hinders reproducibility and impedes independent, large-scale external validation by the research community.

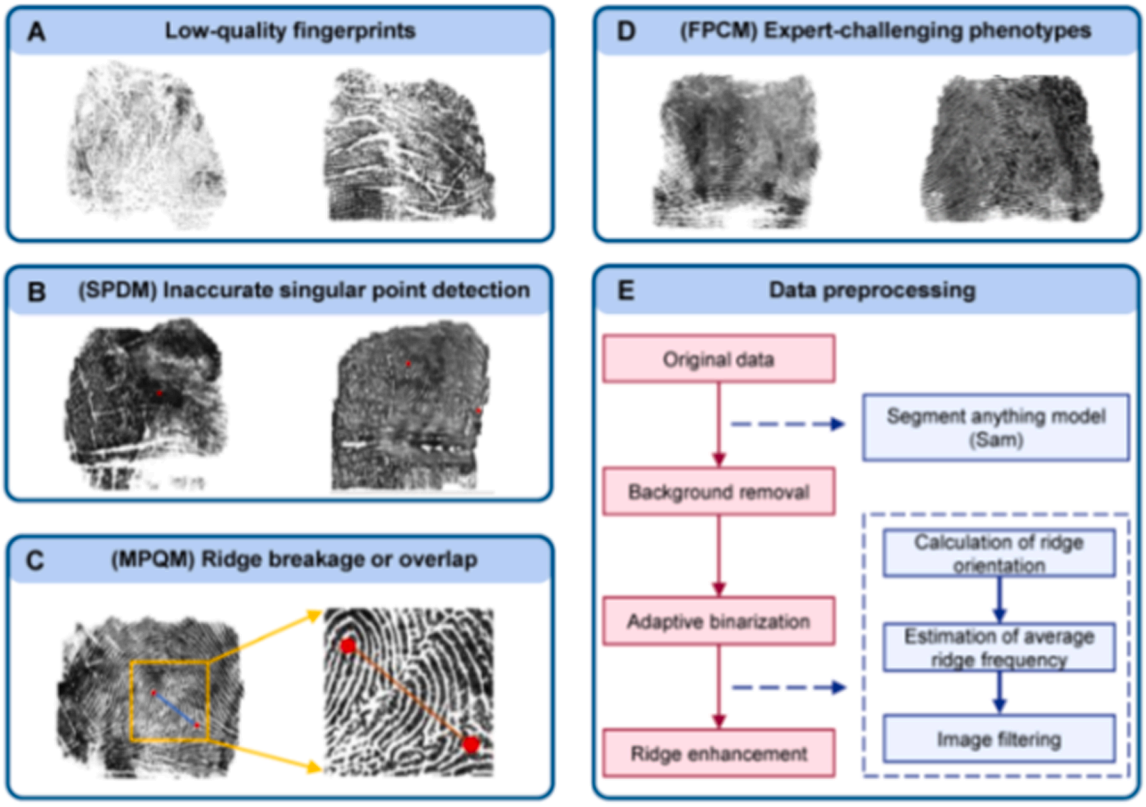

Fig. 7. Scenarios that potentially lead to quantification bias. **(A)** Low-quality fingerprint acquisition with issues such as blurriness and missing parts; **(B)** Inaccurate detection of singular points due to unclear scanning in the core or delta region of the image; **(C)** The ridge counting deviation may be affected by ridge breaks or overlaps; **(D)** Unclear or undistinctive classification. The left image could be interpreted as either a loop or a simple whorl, while the right fingerprint might be classified as an arch or a loop; **(E)** Traditional image-processing-based preprocessing pipeline for domain adaptation, incorporating background removal, adaptive binarization, and ridge enhancement. In this study, the pipeline was applied exclusively to NIST-4 to alleviate domain shift from NSPT.

Second, sensitivity to image quality and domain shift: FPQuant's performance is susceptible to fingerprint image quality and cross-domain discrepancies. Artifacts such as excessive darkness from sweating, incomplete singular points, or pressure distortions (Fig. 7A-C) can adversely affect pattern classification, singularity detection, and ridge counting. Although these low-quality images only constituted 1 % of the total entire private test dataset, they account for approximately 4 % of all misclassifications. This not only highlights their disproportionate and non-negligible impact on model errors but also suggests that the majority of misclassifications likely stem from other, more complex factors, such as techniques or potential data imbalance.

To mitigate both image-quality limitations and domain shift between rolled-scanned images in NSPT and flat-scanned inked pression in NIST-4, we implemented and evaluated a traditional image-processing pipeline incorporating background removal [36], adaptive binarization, and ridge enhancement (Fig. 7E). While this approach exhibits progressive improvements in cross-domain classification accuracy on NIST-4 from 54.05 % to 83.7 %, future work may explore even more lightweight processing—such as denoising and contrast adjustment—to better handle acquisition noise and suboptimal contrast, offering a promising direction for further robustness and applicability gains in diverse challenging real-world environments. It is also noteworthy that the successful efforts made by fine-tuning in model training stage, achieving the highest five-class classification accuracy of 96.20 %, demonstrating it offers a superior solution when sufficient target-domain data are available. Whereas, in data-limited scenarios where fine-tuning is infeasible, the preprocessing pipeline serves as an effective alternative for domain adaptation, significantly improving cross-dataset performance.

Third, inherent class ambiguity and imbalance: classification errors also arise from two other reasons: the one is distinguishing between fine-grained subclasses, such As versus At and Ws versus Wd, proves exceedingly challenging, even for experienced human experts (Fig. 7D), as documented in benchmark datasets such as NIST-4 [24]. These ambiguous cases accounted for 52.5 % of all misclassifications in our dataset. The other one reason is the substantial class imbalance in types, with only approximately 6 % of patterns belonging to the simple arch and tented arch types. Although we employed transfer learning, focal loss, and rotation-based data augmentation to alleviate this, performance on under-represented classes (e.g., Wd) remains suboptimal. The potential future strategies—such as synthetic data generation via generative models (e.g., GANs or diffusion models), virtual sample creation, and advanced ensemble learning [37,38] or multi-objective optimization approaches [39]—may help address severe class imbalance and improve overall robustness across all categories.

6. Conclusion

This study has introduced FPQuant, a unified multi-task deep learning framework for automated and comprehensive fingerprint phenomics quantification like biologically stable features extraction. FPQuant integrates high-accuracy multiple-class fingerprint pattern classification (>98 %), high-precision singular point detection (98.63 %), and fine-grained and expert-comparable morphometric analysis within a single architecture, achieving state-of-the-art performance across multiple benchmarks. Notably, FPQuant integrates a subpixel-level singularity detection module within a unified multi-task architecture, delivering higher localization precision, faster computation, and integrated morphometric analysis compared to existing methods. The framework demonstrates strong cross-database generalizability, maintaining 96.20 % accuracy on NIST-4 and 97.75 % singularity precision on FVC2002 DB1. Critically, FPQuant has uncovered previously uncharacterized geographic variations in fingerprint morphology through its precise quantification of 12 morphometric traits, establishing novel morphometric biomarkers for population genetics and anthropological research.

While the framework incorporates adaptive preprocessing and a strategically designed architecture to enhance robustness, it remains sensitive to image quality, dataset class imbalance, and challenging capture conditions. Its generalizability across diverse ethnic populations also requires further validation. Addressing these aspects including cross-domain adaptation, generative model-based synthetic data generation for rare classes, and expansion to multi-ethnic cohorts remain technical focus for future work to improve generalizability under real-world conditions. In parallel, FPQuant bridges computational pattern recognition and dermatoglyphic science, enabling large-scale reproducible analysis. This paves the way for scientific inquiries into the genetics and development of fingerprint morphology, and supports advanced applications in forensics and precision biometrics.

Ethics statement

All participants provided written informed consent, and all study protocols were approved by the institutional review boards of the pertinent research institutions. The fingerprint dataset of this paper comes from the National Survey of Physical Traits (NSPT), a subject of The National Science & Technology Basic Research Project which was approved by the Ethics Committee of Human Genetic Resources of School of Life Sciences, Fudan University, Shanghai (14,117).

Consent to participate

Written informed consent was obtained from each of the volunteers.

Consent to publication

All the participants approved to publish the paper.

Data and code availability

The NSPT dataset contains sensitive biometric information and is protected under ethical approval (No. 14,117) from the Ethics Committee of Human Genetic Resources, Fudan University; it is not publicly available due to informed consent and privacy regulations. The complete codebase is available at https://github.com/ZhiyongHan-Fudan/FPQuant/tree/main. Data access requests may be directed to the lead contact for consideration under ethical review.

CRediT authorship contribution statement

Zhiyong Han: Writing – original draft, Investigation, Data curation. **Yelin Shi:** Writing – original draft, Investigation, Data curation. **Zhao Zhang:** Writing – review & editing. **Mu Li:** Writing – review & editing. **Haiguo Zhang:** Investigation, Data curation. **Jingze Tan:** Investigation, Data curation. **Wentian Zhen:** Validation, Software. **Tingting Liu:** Validation, Software. **Xueying Wang:** Validation, Software. **Chengyan Wang:** Supervision. **Jiucun Wang:** Supervision. **Li Jin:** Supervision. **Sijia Wang:** Resources, Project administration, Conceptualization. **Manhua Liu:** Resources, Project administration, Conceptualization. **Jinxi Li:** Resources, Project administration, Conceptualization.

Declaration of competing interest

All of authors declare no competing interests.

Acknowledgments

We gratefully acknowledge the participants of the fingerprint dataset who consented to participate in study. This project was supported by the National Natural Science Foundation of China (32200482, 32571342), Shanghai Municipal Science and Technology Major Project (2023SHZDZX02 and 2017SHZDZX01), Shanghai Science and Technology Commission Excellent Academic Leaders Program

(22XD1424700). We thank the Human Phenome Data Center of Fudan University and the Computing for the Future at Fudan (CFFF) platform for their assistance with data acquisition and processing.

Supplementary materials

Supplementary material associated with this article can be found, in the online version, at doi:10.1016/j.patcog.2025.112808.

Data availability

Data will be made available upon reasonable request under a controlled-access agreement.

References

[1] H.S. Kahn, M. Graff, A.D. Stein, P.A. Zybert, I.W. McKeague, L.H. Lumey, A fingerprint characteristic associated with the early prenatal environment, Am. J. Hum. Biol. 20 (2008) 59–65.
[2] J. Li, J.D. Glover, H. Zhang, M. Peng, J. Tan, C.B. Mallick, D. Hou, Y. Yang, S. Wu, Y. Liu, Q. Peng, S.C. Zheng, E.I. Crosse, A. Medvinsky, R.A. Anderson, H. Brown, Z. Yuan, S. Zhou, Y. Xu, J.P. Kemp, Y.Y.W. Ho, D.Z. Loesch, L. Wang, Y. Li, S. Tang, X. Wu, R.G. Walters, K. Lin, R. Meng, J. Lv, J.M. Chernus, K. Neiswanger, E. Feingold, D.M. Evans, S.E. Medland, N.G. Martin, S.M. Weinberg, M.L. Marazita, G. Chen, Z. Chen, Y. Zhou, M. Cheeseman, L. Wang, L. Jin, D.J. Headon, S. Wang, Limb development genes underlie variation in human fingerprint patterns, Cell 185 (2022) 95–112.
[3] A. Peng, R. Huang, Research progress on the application of deep learning in fingerprint recognition, Pattern. Recognit. 171 (2026) 112216.
[4] M.A. Acree, Is there a gender difference in fingerprint ridge density? Forensic Sci. Int. 102 (1999) 35–44.
[5] H.-G. Zhang, Y.-F. Chen, M. Ding, L. Jin, D.T. Case, Y.-P. Jiao, X.-P. Wang, C.-X. Bai, G. Jin, J.-M. Yang, Dermatoglyphics from all Chinese ethnic groups reveal geographic patterning, PLoS One 5 (2010) e8783.
[6] I. Singh, P.K. Chattopadhyay, R.K. Garg, Determination of the hand from single digit fingerprint: a study of whorls, Forensic Sci. Int. 152 (2005) 205–208.
[7] F. Wu, J. Zhu, X. Guo, Fingerprint pattern identification and classification approach based on convolutional neural networks, Neural Comput. Appl. 32 (2020) 5725–5734.
[8] A.B. Mokal, B. Gupta, A deep learning approach for effective classification of fingerprint patterns and human behavior analysis, Pattern. Recognit. 163 (2025) 111439.
[9] E.-S.-M. El-kenawy, A. Ibrahim, S. Mirjalili, Y.-D. Zhang, S. Elnazer, R.-M. Zaki, Optimized ensemble algorithm for predicting metamaterial antenna parameters, Comput. Mater. Contin. 71 (2022) 4989–5003.
[10] E.-S.M. El-Kenawy, N. Khodadadi, S. Mirjalili, T. Makarovskikh, M. Abotaleb, F. K. Karim, H.K. Alkahtani, A.A. Abdelhamid, M.M. Eid, T. Horiuchi, A. Ibrahim, D. S. Khafaga, Metaheuristic optimization for improving weed detection in wheat images captured by drones, Mathematics 10 (2022) 4421.
[11] D. Michelsanti, A.-D. Ene, Y. Guichi, R. Stef, K. Nasrollahi, T.B. Moeslund, Fast fingerprint classification with deep neural networks, in: International Conference on Computer Vision Theory and Applications, Scitepress, 2017, pp. 202–209.
[12] P. Akhila, S.G. Koolagudi, Hand classification based on fingerprint using Lightweight Convolutional Neural Network, in: 2025 IEEE Guwahati Subsection Conference (GCON), IEEE, 2025, pp. 1–6.
[13] Y. Fan, J. Li, S. Song, H. Zhang, S. Wang, G. Zhai, Palmprint phenotype feature extraction and classification based on deep learning, Phenomics 2 (2022) 219–229.
[14] J. Zhou, F. Chen, J. Gu, A novel algorithm for detecting singular points from fingerprint images, IEEE Trans. Pattern. Anal. Mach. Intell. 31 (2008) 1239–1250.
[15] J. Qin, C. Han, C. Bai, T. Guo, Multi-scaling detection of singular points based on fully convolutional networks in fingerprint images, in: J. Zhou, Y. Wang, Z. Sun, Y. Xu, L. Shen, J. Feng, S. Shan, Y. Qiao, Z. Guo, S. Yu (Eds.), Biometric Recognition, Springer International Publishing, Cham, 2017, pp. 221–230.
[16] Y. Liu, B. Zhou, C. Han, T. Guo, J. Qin, A method for singular points detection based on faster-RCNN, Appl. Sci. 8 (2018) 1853.
[17] G. Arora, A. Kumbhat, A. Bhatia, K. Tiwari, CP-Net: multi-scale core point localization in fingerprints using hourglass network, in: 2023 11th International Workshop on Biometrics and Forensics (IWBF), 2023, pp. 1–6.
[18] A.N. Bonacim, R. Minetto, M.P. Segundo, Machine learning for fingerprint ridge counting, IEEE Trans. Biom. Behav. Identity Sci. (2025), 1-1.
[19] T. Jiang, P. Lu, L. Zhang, N. Ma, R. Han, C. Lyu, Y. Li, K. Chen, Rtmpose: real-time multi-person pose estimation based on mmpose, arXiv preprint arXiv:2303.07399, (2023).
[20] A. Torralba, B.C. Russell, J. Yuen, Labelme: online image annotation and applications, Proc. IEEE 98 (2010) 1467–1484.
[21] K.A. Kamp, N. Timmerman, G. Lind, J. Graybill, I. Natowsky, Discovering childhood: using fingerprints to find children in the archaeological record, Am. Antiq. 64 (1999) 309–315.
[22] R. Syam, M. Hariadi, M.H. Purnomo, Determining the dry parameter of fingerprint image using clarity score and ridge-valley thickness ratio, Iaeng Int. J. Comput. Sci. 38 (2011) 350–358.
[23] N. Rivaldería, A. Moreno-Piedra, A. Álvarez, E. Gutiérrez-Redomero, Study of the fingerprints of a Spanish sample for the determination of the hand and finger, Sci. Justice 64 (2024) 216–231.
[24] C.I. Watson, C.L. Wilson, NIST Special Database 4, (1992).
[25] D. Maio, D. Maltoni, R. Cappelli, J.L. Wayman, A.K. Jain, FVC2002: second fingerprint verification competition, in: Proceedings of the 16 th International Conference on Pattern Recognition (ICPR'02) Volume 3 - Volume 3, 2002.
[26] X. Chen, C. Yang, J. Mo, Y. Sun, H. Karmouni, Y. Jiang, Z. Zheng, CSPNeXt: a new efficient token hybrid backbone, Eng. Appl. Artif. Intell. 132 (2024) 107886.
[27] Y. Li, S. Yang, P. Liu, S. Zhang, Y. Wang, Z. Wang, W. Yang, S.-T. Xia, SimCC: a simple coordinate classification perspective for Human pose estimation, Eds., in: S. Avidan, G. Brostow, M. Cissé, G.M. Farinella, T. Hassner (Eds.), Computer Vision – ECCV 2022, Springer Nature Switzerland, Cham, 2022, pp. 89–106.
[28] T.Y. Lin, P. Goyal, R. Girshick, K. He, P. Dollár, Focal loss for dense object detection, in: 2017 IEEE International Conference on Computer Vision (ICCV), 2017, pp. 2999–3007.
[29] Q. Zhang, H. Yan, Fingerprint classification based on extraction and analysis of singularities and pseudo ridges, Pattern. Recognit. 37 (2004) 2233–2243.
[30] Y. Yao, P. Frasconi, M. Pontil, Fingerprint classification with combinations of Support Vector machines, Eds., in: J. Bigun, F. Smeraldi (Eds.), Audio- and Video-Based Biometric Person Authentication, Springer Berlin Heidelberg, Berlin, Heidelberg, 2001, pp. 253–258.
[31] X. Tan, B. Bhanu, Y. Lin, Fingerprint classification based on learned features, IEEE Trans. Syst. Man Cybern. C (Appl. Rev.) 35 (2005) 287–300.
[32] D. Peralta, I. Triguero, S. García, Y. Saeys, J.M. Benitez, F. Herrera, On the use of convolutional neural networks for robust classification of multiple fingerprint captures, Int. J. Intell. Syst. 33 (2018) 213–230.
[33] J. Zhou, F. Chen, J. Gu, A novel algorithm for detecting singular points from fingerprint images, IEEE Trans. Pattern. Anal. Mach. Intell. 31 (2009) 1239–1250.
[34] J.D. Glover, Z.R. Sudderick, B.B. Shih, C. Batho-Samblas, L. Charlton, A.L. Krause, C. Anderson, J. Riddell, A. Balic, J. Li, V. Klika, T.E. Woolley, E.A. Gaffney, A. Corsinotti, R.A. Anderson, L.J. Johnston, S.J. Brown, S. Wang, Y. Chen, M. L. Crichton, D.J. Headon, The developmental basis of fingerprint pattern formation and variation, Cell 186 (2023) 940–956, e920.
[35] G. Iwasokun, B. Alese, A. Charles, O. Olatubosun, Fingerprint image enhancement: segmentation to thinning, Int. J. Adv. Comput. Sci. Appl. 3 (2012).
[36] A. Kirillov, E. Mintun, N. Ravi, H. Mao, C. Rolland, L. Gustafson, T. Xiao, S. Whitehead, A.C. Berg, W.Y. Lo, P. Dollár, R. Girshick, Segment anything, in: 2023 IEEE/CVF International Conference on Computer Vision (ICCV), 2023, pp. 3992–4003.
[37] R. Alkanhel, E.-S.-M. El-kenawy, A.-A. Abdelhamid, A. Ibrahim, M.-A. Alohali, M. Abotaleb, D.-S. Khafaga, Network intrusion detection based on feature selection and hybrid metaheuristic optimization, Comput. Mater. Contin. 74 (2023) 2677–2693.
[38] E.-S.M. El-kenawy, S. Mirjalili, N. Khodadadi, A.A. Abdelhamid, M.M. Eid, M. El-Said, A. Ibrahim, Feature selection in wind speed forecasting systems based on meta-heuristic optimization, PLoS One 18 (2023) e0278491.
[39] N. Khodadadi, L. Abualigah, E.S.M. El-Kenawy, V. Snasel, S. Mirjalili, An archive-based multi-objective arithmetic optimization algorithm for solving industrial engineering problems, IEEE Access 10 (2022) 106673–106698.